

Performance of large format 2Kx2K MBE grown HgCdTe Hawaii-2RG arrays for low flux applications.

G. Finger*, R. J. Dorn, M. Meyer, L. Mehrgan, J. Stegmeier, A.F.M. Moorwood
European Southern Observatory, Karl Schwarzschildstrasse 2 D-85748 Garching, Germany.

ABSTRACT

VLT instruments increasingly require high sensitivity large format focal planes. Adaptive optics combined with multiple integral field units feeding high resolution spectrographs drive the pixel performance as well as the array format. Three VLT instruments, the wide field imager Hawk-I [1] and the integral field spectrographs SINFONI [2] and KMOS [3] will be equipped with MBE-grown HgCdTe Hawaii-2RG arrays, which have a cut-off wavelength of 2.5 micron. The Hawaii-2RG array was originally developed for the near infrared camera of JWST having a cut-off wavelength of 5 micron [4].

The Hawaii-2RG multiplexer is one of the most advanced readout architectures offering a large variety of operating modes. A special 32 channel package has been developed which allows reading out all 32 output channels of the detector in parallel [7]. Symmetric cryogenic CMOS operational amplifiers are placed next to the focal plane instead of using ASIC's which are not yet available. The internal bus of the detector is accessed directly, bypassing the on-chip buffer amplifier. Noise performance employing different techniques of using reference pixels is discussed. Basic performance characteristics of the Hawaii-2RG arrays will be presented. Unlike LPE arrays, which lose quantum efficiency at lower temperatures, MBE arrays with $\lambda_c=2.5 \mu\text{m}$ do not show this effect. However, the MBE arrays under test still suffer from persistence.

Keywords: infrared detector, Hawaii-2RG, HgCdTe, readout noise, dark current, quantum efficiency, persistence

1. Introduction

In 1997 ESO participated in the funding of the development of Hawaii2 2Kx2K LPE arrays. A science grade array was delivered in 2001. Although in most respects the Hawaii2 science grade array exhibits excellent performance, there are some problems associated with the Hawaii2 multiplexer such as rise times of less than 50 ns for clocks of the fast shift register and the complexity of using the reference output [6]. Consequently, Rockwell redesigned the Hawaii2 multiplexer resulting in the Hawaii-2RG multiplexer, which has different types of reference pixels and a built in guide mode [5]. The growth technology for the infrared diode array has also been changed from liquid phase epitaxy (PACE material) to double layer planar heterostructure HgCdTe arrays grown by molecular beam epitaxy on CdZnTe substrates[4]. In comparison to PACE material this technology has lower defect densities. As a consequence, the detector dark current is reduced substantially and the array can be operated at higher temperatures. This growth process also showed great promise to reduce the persistence effect. This cannot be fully confirmed yet. ESO has received two engineering grade Hawaii-2RG arrays. Both of these arrays exhibit reduced, but non-negligible persistence.

2. Set-up

Because of stringent power limitations on JWST, which is one application for the Hawaii2-RG detectors, only four channels of the array are read out in parallel resulting in a minimum integration time of 41 seconds. This readout time is too long for ground based applications. For this reason a joint effort was made by Gemini, Keck, CFHT and ESO to fund GL Scientific to develop the 32-channel detector package interfacing all 32 video channels of the Hawaii-2RG multiplexer. The backside of the 32-channel detector package is shown in Figure 1 with the flex board mounted on the PGA [7]. At the end of the flex board there is a 92 pin HIROSE connector for electrical interfacing. The array is

* gfinger@eso.org, phone:+49-89-32006256, :+49-89-3200316, fax:+49-89-3202362

mounted on a molybdenum supporting structure. Molybdenum has been chosen because it best matches the thermal expansion coefficient of HgCdTe and minimizes stress during cooldown. Thermal contact to the base plate is made via the molybdenum spacers and the four Cu/W mounting pins of the detector package. Four mounting points are used to ensure that the thermal contact is symmetrically distributed in the detector package.

Two set-ups are used for the Hawaii-2RG detectors at ESO, one for instruments housing a single detector and one for applications needing a close buttable mosaic of four Hawaii-2RG arrays. Both set-ups utilize all 32-video channels offered by the detector. The fan-out board for the mosaic contains cryogenic preamplifiers for the 136 channels of the four detectors, filters for clock and bias voltages as well as antistatic protection circuits. Two engineering grade arrays have already been delivered in the 32-channel package.

The single detector mount with three alignment screws for tip-tilt and focus alignment is shown on the right side of Figure 1. The detector is mounted on an aluminium detector base plate supported by an epoxy frame and cooled by a massive copper cold finger on the backside (Figure 2). This copper block is heat-sunk by a flexible copper strap to the second stage of a pulse tube closed cycle cooler. The Al base plate is flexured at one of the hole locations by two slits so that the detector is not over-constrained when pulled down onto the base plate. On the side of the detector mount the detector board houses the cryogenic preamplifiers for 32 video channels plus one reference channel and one extra channel for the guiding window (see Figure 2).

For JWST a buttable 2x2 2Kx2K Hawaii-2RG mosaic package has been developed to equip the focal plane of NIRCAM. A mount designed by GL Scientific is shown in Figure 3 [7]. This mosaic module is used by several astronomy groups. To avoid duplication of efforts and share development costs and nonrecurring expenses, it was decided to procure the complete mosaic module from GL Scientific. The co-planarity of the four arrays is managed by the thickness of the molybdenum spacers. In Hawk-I the focal ratio at the detector is $f/3.8$. The co-planarity misalignment has to be smaller than $\pm 20 \mu\text{m}$ to keep the image blur below $5 \mu\text{m}$ or 25% of the pixel size. The active area of the array does not extend to the edge of the multiplexer. 4 rows and columns of reference pixels, two vertical and horizontal shift registers, amplifiers and interconnection lines have to be accommodated between the active area and the edge of the multiplexer. The minimum spacing between the active area of two arrays must be 2.65 mm at least, or 147 pixels. The area required for the fan-out board serving all four detectors is estimated to be 8 cm x 8 cm which is larger than the area provided for the four SIDECAR ASIC's of the JWST module and slightly larger than the area of the detector mosaic but should still fit into the space envelope of the GL Scientific package foreseen for the ASIC's [9].

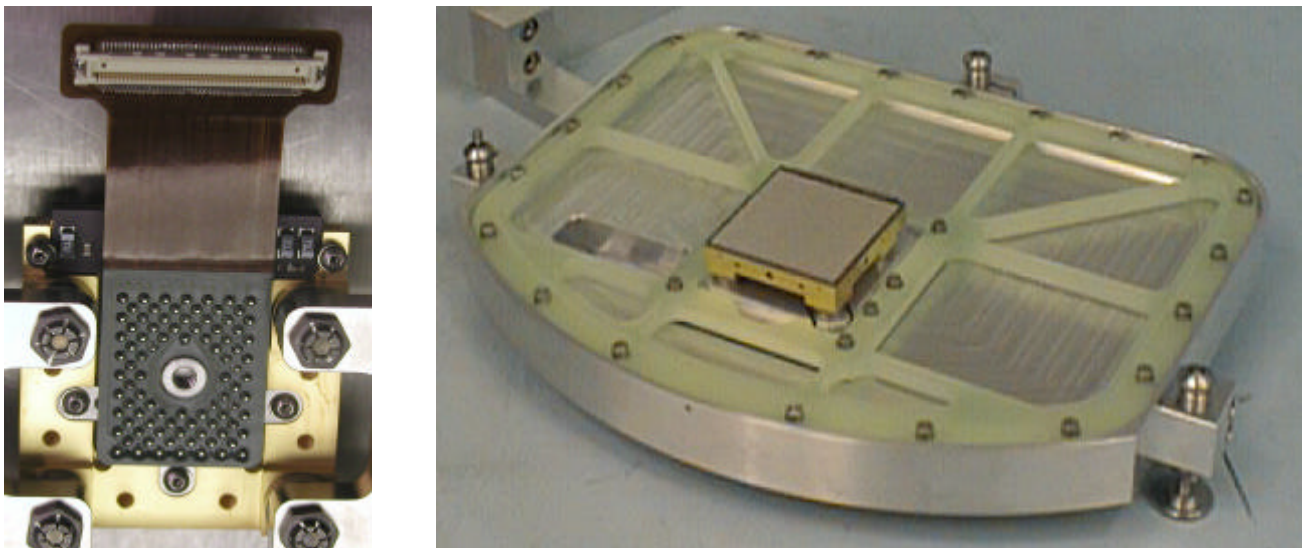


Figure 1 Left: Hawaii-2RG array in 32 channel package with flex board and 92-pin HIROSE connector. Right: Hawaii-2RG bare multiplexer mounted on SPIFFI detector mount with three alignment screws for tip-tilt and focus alignment.

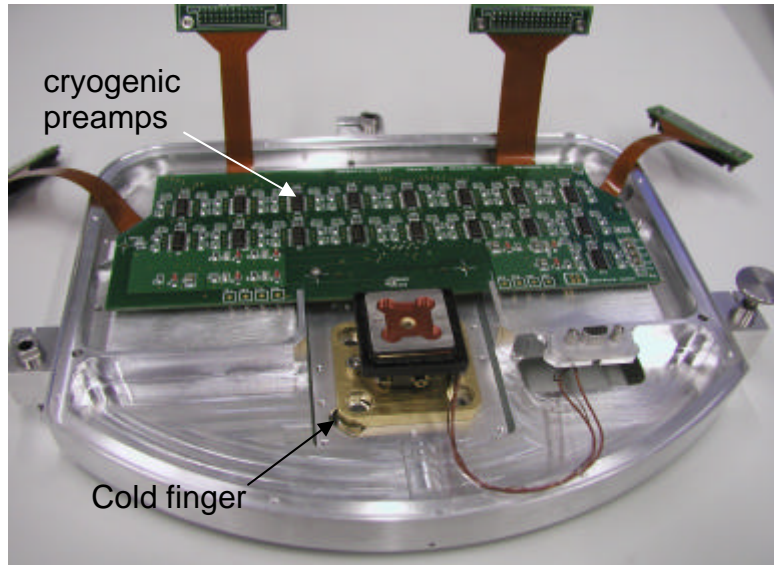


Figure 2 Hawaii-2RG detector mount for SPIFFI with cryogenic preamplifiers for 32 video channels plus one reference channel and one extra channel for guiding window.

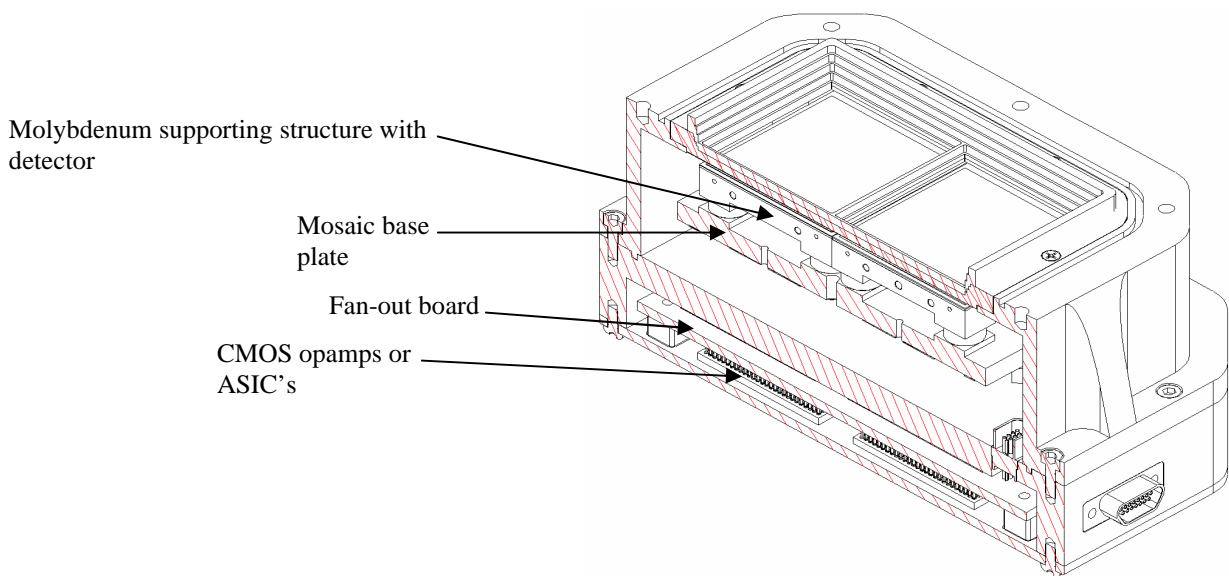


Figure 3 GL Scientific Hawaii2RG mosaic module

3. Thermal behavior of cryogenic preamplifiers

The power dissipation of the preamplifier consisting of 68 CMOS operational amplifiers (2/channel) is ~ 1 W. In comparison, the power dissipation of the detector using the unbuffered outputs is negligible (~ 10 mW, $300\mu\text{W}/\text{channel}$). Thus, in the vicinity of the detector the main heat source is constituted by the preamplifiers. This puts a certain heat load on the detector. In order to quantify the heat load of the preamplifiers and the effect on the performance of the detector two experiments were performed. In the first test the detector temperature was measured during normal operation while the heater of the detector temperature control loop was switched off. With zero heating

power the detector temperature stabilized at 34.5K. Then the detector and the preamplifiers were switched off and the heating power was measured to keep the detector at the same temperature. The heating power was 230 mW. Since the power dissipation of the preamplifiers for a single detector is 1 W, the heat load on the detector and the second stage of the closed cycle cooler is only 23 % of the total power dissipated by the preamplifiers. The main portion is heat-sunk to the instrument and the first stage of the closed cycle cooler. For this reason it is important to redirect the major fraction of the heat flow to the instrument by a thermal clamp of the detector cables, which is located close to the preamplifier board. In the second test the rail voltage of the cryogenic opamps was reduced from its nominal 6 V to 3 V and the dark current was measured. Within the accuracy of the measurement no reduction of the dark current could be observed. A temperature sensor glued onto one of the operational amplifiers showed a temperature of 150 K for a rail voltage of

6 V. At this temperature the photon flux seen by a $\lambda_c=2.6 \mu\text{m}$ cut-off detector is 0.1 photons/s/pixel assuming a solid angle of 2π steradian. Moderate baffling corresponding to $f/10$ reduces the flux generated by thermal emission of the CMOS opamps to negligible levels of $2 \cdot 10^{-4}$ e/s/pixel.

As far as possible, the cryogenic design features of the single detector set-up shall be ported to the mosaic provided by GL-scientific. Since the GL-scientific set-up was designed for small low power ASIC's the ESO preamplifier board shall be mounted with minimum thermal contact to the mosaic enclosure, which is at detector temperature. Epoxy mounting studs shall be used. The cable feed-throughs shall minimize the thermal contact to the detector enclosure. The emissivity of the preamplifier enclosure shall be high to baffle thermal radiation.

4. Quantum efficiency

The temperature dependence of the quantum efficiency of the engineering grade array was measured in the J, H and K bands. The QE was measured both by imaging an extended blackbody onto the detector and by illuminating the detector without re-imaging optics using defined entendues $\Delta\Omega$ in both cases. The results agree within 4%. The temperature

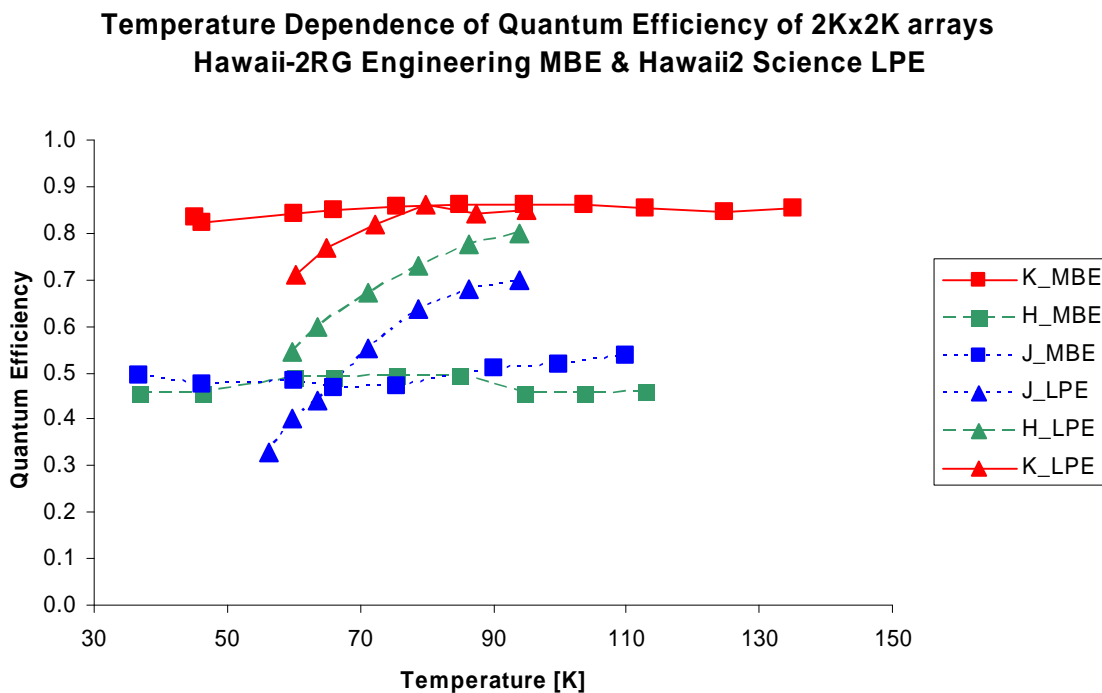


Figure 4 Temperature dependence of quantum efficiency. Squares: Hawaii-2RG MBE on CdZnTe. Triangles: Hawaii2 LPE on Al_2O_3 . Solid lines: K. Dashed lines: H. Dotted lines: J.

dependence of the quantum efficiency of the MBE Hawaii-2RG engineering grade array is represented by squares in Figure 4 and compared to the quantum efficiency of the Hawaii2 science grade array, which is based on LPE material grown on sapphire. In the K band the high quantum efficiency of the MBE array is outstanding at low temperatures, but the QE drops to below 0.5 in the H and J band. For this reason the array was classified as engineering grade. The QE of MBE material does not depend on temperature whereas the QE of LPE material drops at lower temperatures. Hence, for MBE arrays the cosmetic performance, which improves rapidly at lower temperatures, can be enhanced by reducing the operating temperature without loss of quantum efficiency.

5. Readout Noise

The readout noise for simple double correlated sampling is 17 electrons rms for infrared active pixels. The infrared active pixels of the Hawaii-2RG array are surrounded by 4 rows and columns of reference pixels at the edges of the array. The signal of these pixels is embedded in the regular video signal of 2048 x 2048 pixels. Therefore, the active area consists of 2040 x 2040 light sensitive pixels. The reference pixels can be used to track low frequency noise pick-up. Unlike standard infrared-active pixels, the reference pixels are not connected to detector photodiodes. Instead, they contain a simple capacitor C_{pix} whose capacitance is similar to the detector capacitance. The readout noise measured on these reference pixels at the edges of the array is only 8 electrons rms. This proves that the contribution of the readout multiplexer and the rest of the data acquisition chain including the preamplifiers and the IRACE electronics to the overall readout noise is small. The readout noise is dominated by the noise of the infrared pixel. Figure 5 shows a noise map at the edge of the array. The darker left four columns at the left edge of the array are reference pixels.

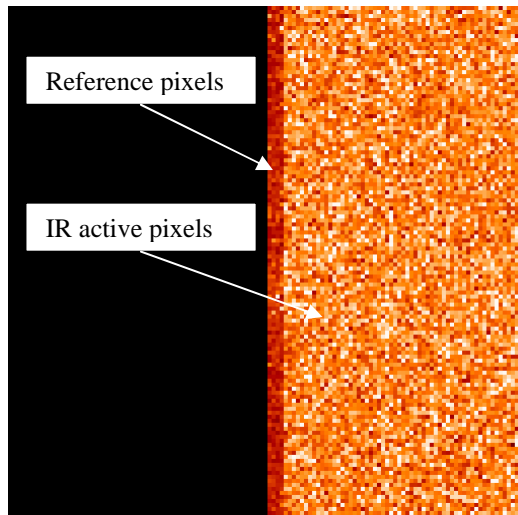


Figure 5 Noise map with reference pixels at the left edge. Readout noise on active pixels: 17 erms. Readout noise on reference pixels at left edge: 8 erms.

6. Embedded reference pixels

Although the cryo-opamps on the ESO detector board have all provisions to test the separate reference output, so far only embedded reference pixels have been tested. Since all 32 channels are used and the array is organized in stripes which are 2048 rows long, the rows of a single stripe contain only 64 pixels. If the array is read out at a frame rate of 1.2 Hz the reference pixels are read every 400 μ s, which is the time needed to read a single row. The squared transfer function of a double correlated clamp is $2-2\cos(2\pi ft_s)$. For a pickup frequency of 50Hz and a sampling interval t_s of 400 μ s between reading the pixel and reading the reference, in the worst case the transfer function will be 0.125, which is the suppression factor for 50Hz pickup. For the images shown in Figure 6 the integration time was intentionally set to 1.01 s

which is not a multiple of 20 ms. This was done to demonstrate the reduction of 50 Hz pick-up by the use of embedded reference pixels. The left image is the difference of two images taken with double correlated sampling. The 50Hz pick-up contained in the image increases the pixel to pixel standard deviation to 45 erms. In the middle image the mean of the reference pixels of a particular row at the right and at the left edge of the array was subtracted from each pixel in the row which is very effective in removing low frequency noise components and reduces the read noise to 25 erms. The white noise increase induced by subtraction is only 6% since 8 embedded reference pixels are averaged. The average value of the reference pixels is then subtracted from the signal of each pixel. Linear interpolation between two average values of reference pixels, the average of the reference pixels of the row just being read and the average of the reference pixels of the next row, slightly improves the removal of pick-up components and yields uniform white noise images as shown in the right image of Figure 6 [8]. The pixel to pixel standard deviation is reduced to 23 erms. Since the horizontal readout direction of each stripe of the Hawaii-2RG multiplexer can be controlled and two adjacent stripes have opposite readout directions for the settings used here, reference pixels of adjacent rows have to be used for linear interpolation. If all stripes are clocked in the same horizontal direction, the left four and the right four reference pixels of the same row can be used for linear interpolation. This mode is still to be tested. Most of the low frequency noise sources V_i are capacitively coupled into the integrating node capacity C , which is assumed to be large in comparison to the coupling capacities C_i . The coupling constant for the noise source V_i is C/C_i . Since the pick-up is well removed the capacity connected to the gate of the reference cells is well matched to the capacity of the infrared diodes.

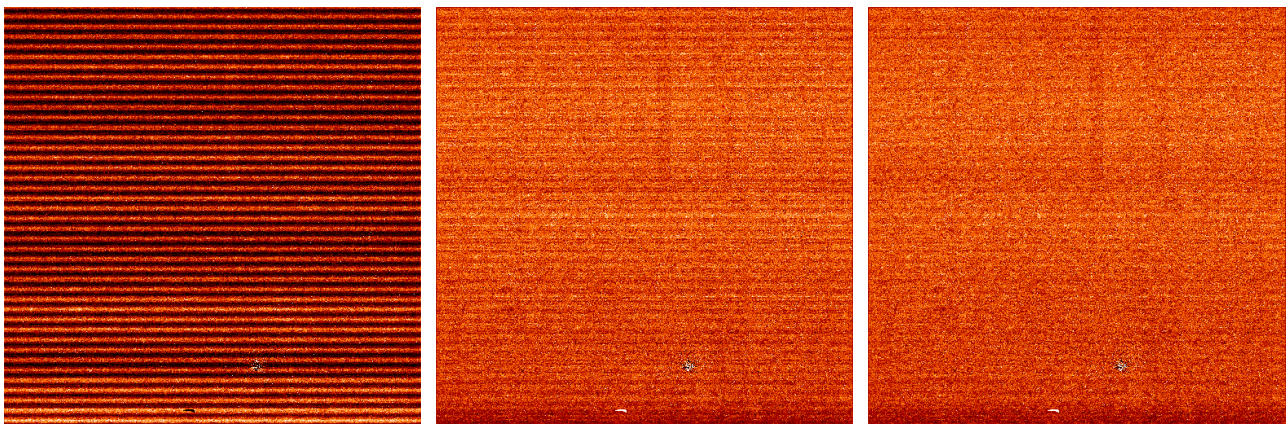


Figure 6 Difference images of double correlated clamps corrected with reference pixels at left and right edges of array which are embedded in regular video data stream. Left image: Uncorrected showing 50Hz pick-up. Middle image: corrected with mean of reference pixels subtracted. Right image: Corrected with linear interpolation of reference for each IR-active pixel using reference pixels of row next row.

7. Multiple sampling techniques

Multiple sampling techniques substantially reduce the readout noise as can be seen in Figure 7 which shows the readout noise versus the number of nondestructive readouts. Active infrared pixels are represented by squares, reference pixels by triangles. Noise measurements taken at ESO and plotted as solid lines are compared with measurements taken at STScI represented by dashed lines in Figure 7 [10]. The readout time for a single non-destructive readout is 825 ms and the detector is continuously read out. The detector integration time for 2048 readouts is 845 seconds. The lowest readout noise on the active IR pixels is 3 erms with 256 Fowler pairs, the lowest readout noise on reference pixels is 1.8 erms. In Figure 8 a noise histogram of the infrared active pixels is shown for 256 Fowler pairs (512 nondestructive readouts)

This outstanding noise performance impressively demonstrates two accomplishments of the Hawaii-2RG multiplexer design. First, the shielding of the multiplexer glow, which because of glow-induced photon shot noise limited the number of Fowler pairs to < 32 with previous multiplexers, has been implemented very efficiently in the Hawaii-2RG device. Second, the implementation of 32 parallel video channels not only reduces the readout time, but, which is more

important, also improves the noise performance, since more non-destructive readouts can be made within a given integration time. This results in a further reduction of the readout noise.

The shielding of the multiplexer glow is not perfect. For larger numbers of nondestructive readouts a few localized glow centers appear at random locations across the array. The glow centers have a ring-like structure and a diameter of ~ 12 pixels as shown in Figure 9. The intensity of the glow centers depends on the number of nondestructive readouts and on the operating temperature, as can be seen in Figure 10. Cooling the array to lower temperatures decreases the intensity of the glow centers. At temperatures below 60 K the glow centers disappear.

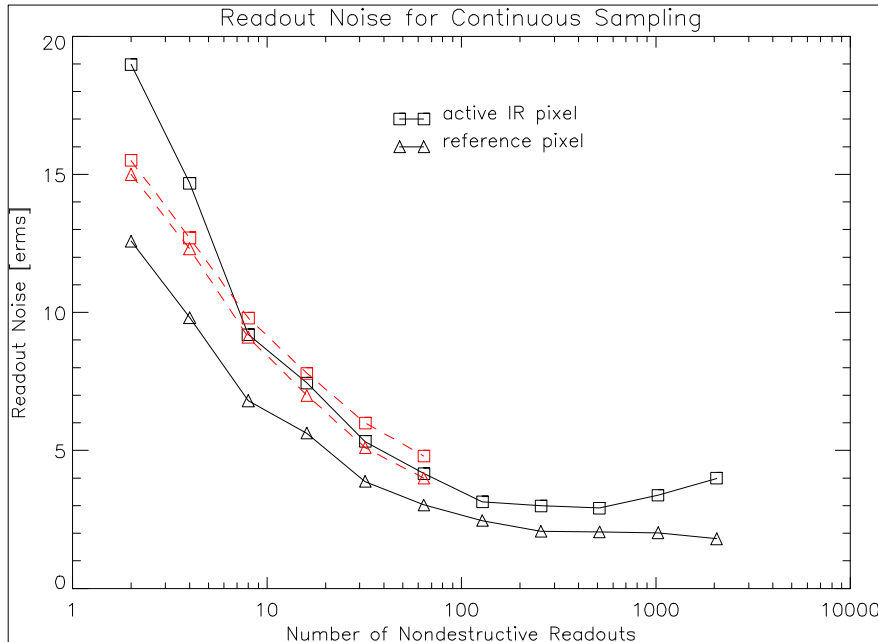


Figure 7 Readout noise versus number of nondestructive readouts. Squares: active infrared pixels. Triangles: reference pixels. Solid line: ESO data. Dashed line: STScI data for comparison. Readout time for single readout: 825 ms. Lowest readout noise on active IR pixel: 3erms with 256 Fowler pairs. Lowest readout noise on reference pixels: 1.8 erms.

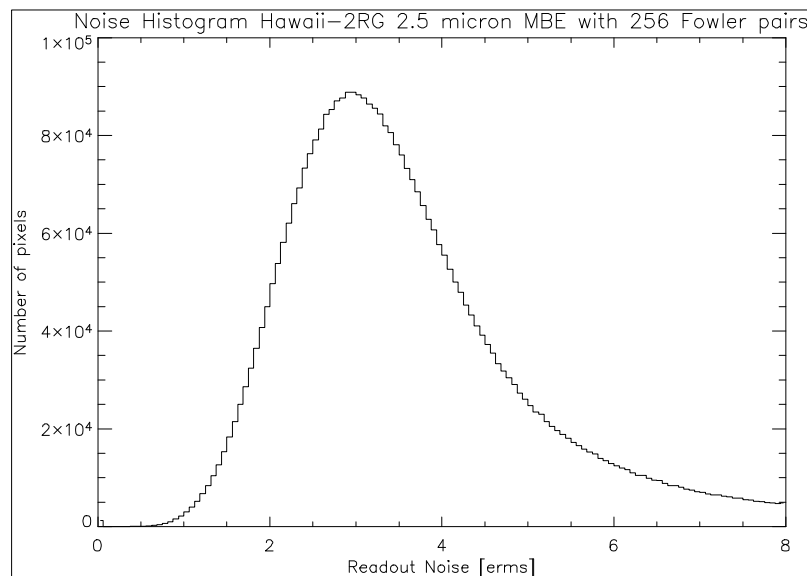


Figure 8 Histogram of readout noise on infrared active pixels of Hawaii-2RG array with 256 Fowler pairs. Readout Noise is 3 electrons rms.

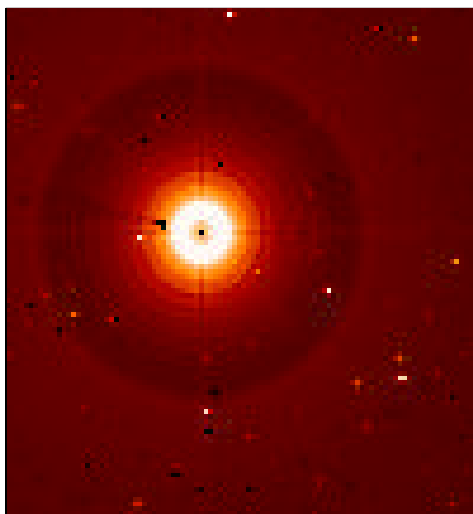


Figure 9 Glow center for 2048 nondestructive readouts at temperature of 50 K.

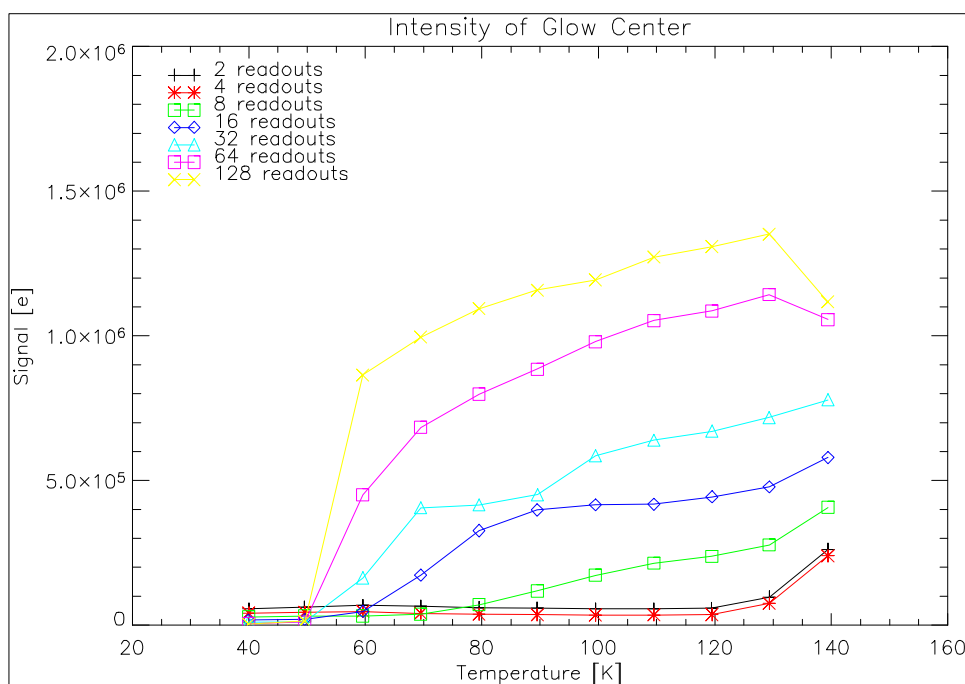


Figure 10 Intensity of glow center versus temperature for varying number of readouts. Integration time fixed at 60 seconds.

8. Darkcurrent

The darkcurrent of the $\lambda_c=2.5 \mu\text{m}$ Hawaii-2RG MBE/CdZnTe array was measured in a test facility equipped with a two stage pulse tube to cool the detector. For dark current measurements the detector was completely enclosed in a black anodized aluminum box. Thus, the instrumental photon background caused by imperfect radiation shielding of the test facility is not seen by the detector. The dark current is $< 0.01 \text{ e/sec}$ at temperatures below 80 K in clean regions of the array as shown by the filled triangles in Figure 11. For comparison the darkcurrent measured with a $\lambda_c=2.5 \mu\text{m}$ Hawaii2 LPE/ Al_2O_3 science grade array (filled squares in Figure 11), a Hawaii1 LPE/ Al_2O_3 science grade array (squares in

Figure 11), and a $\lambda_c=1.7 \mu\text{m}$ PICNIC MBE/CdZnTe array (triangles) are shown as well. The darkcurrent of the PICNIC array was scaled to the pixel size of $18 \mu\text{m}$. At an operating temperature of 100K the darkcurrent of MBE/CdZnTe arrays with $\lambda_c=2.5 \mu\text{m}$ is a factor of 1660 times lower than that of LPE/ Al_2O_3 arrays. This improvement is of particular importance for instruments which do not have closed cycle coolers but have to manage with liquid nitrogen bath cryostats.

In regions of the MBE array exhibiting high dark current, cooling the array below 80 K further reduces the dark current. The improvement of the cosmetic appearance for lower temperatures is shown in a series of dark exposures in Figure 12, displaying the full $2\text{K} \times 2\text{K}$ frames, and in Figure 13 which shows a region of high dark current. If the science grade array is perfect and does not have any regions of excess dark current it can be operated at 80 K. However, high dark current areas of the array improve when cooled to lower temperatures.

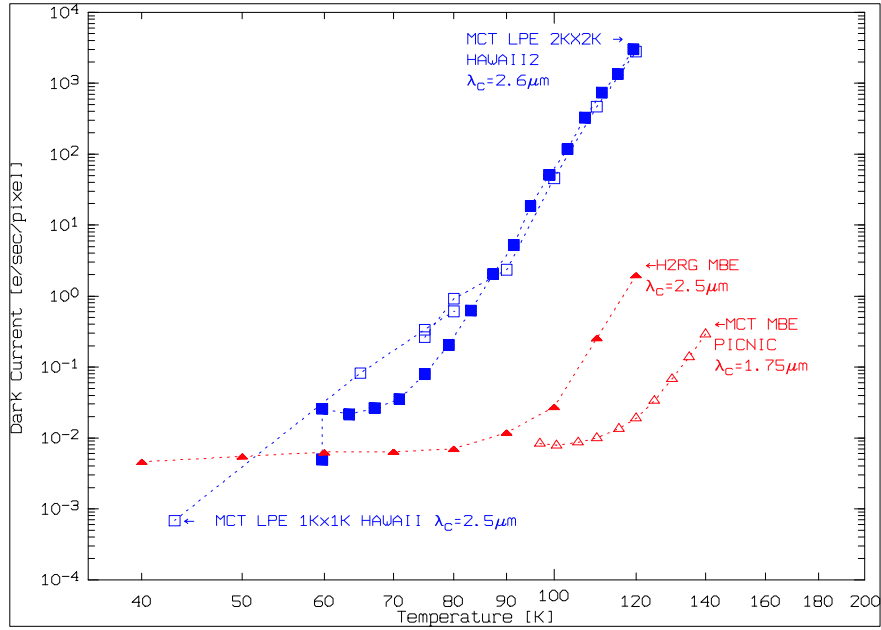


Figure 11 Dark current versus temperature for HgCdTe arrays. Squares: LPE material. (squares: Hawaii1 1Xx1K, filled squares: Hawaii2 2Kx2K) . Triangles: MBE on CdZnTe substrate. (filled triangles: Hawaii-2RG engineering grade array, triangles: $\lambda_c=1.7 \mu\text{m}$ PICNIC).

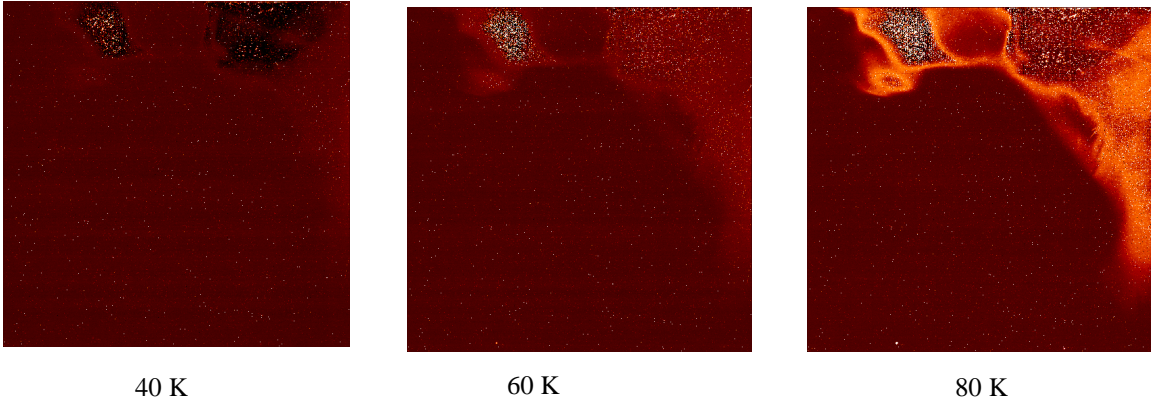


Figure 12 Dark current maps of Hawaii-2RG engineering grade array #9 for different temperatures. Cut levels $-0.5 / 2 \text{ e/sec}$. Integration time 11 minutes.

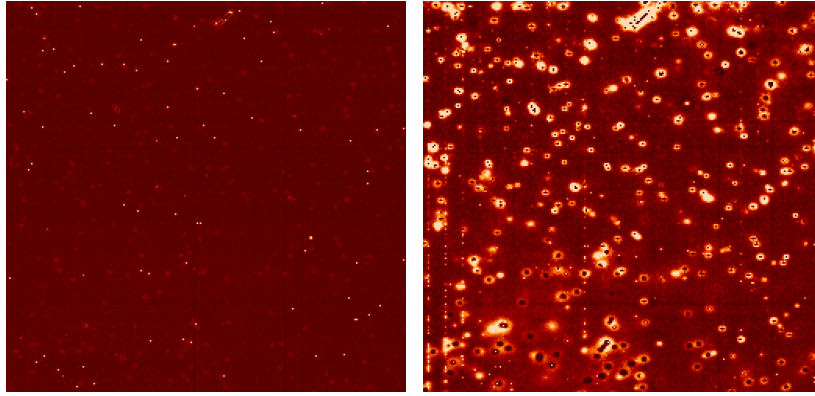


Figure 13 Comparison of cosmetic quality in high dark current region. Left:40 K. Right: 80K.Cut levels: -250 /2000 e. Integration time: 900 sec

9. Persistence

Latent charge, or “persistence,” is the remaining signal apparent in a series of dark exposures. It is produced by a bright source in previous images where the detector was exposed to high photon flux levels. Any process which, after some delay, releases charge into the conduction band can contribute to latent charge. The latent charge can be caused by a bright star or a cosmic ray. Latent charge is a function of incident flux during a previous exposure, the time elapsed since the previous exposure, the applied reverse bias on the unit cell, and the temperature.

To examine the latent image effect, a blackbody was imaged onto the detector through the J-band filter. The blackbody was set to a temperature of 320 Celsius which left the detector completely saturated, while a series of 20 second exposures was taken at an operating temperature of 70K. The filter wheel was then set to the dark position. The flux of the latent images apparent in the subsequent 20 second dark exposures is plotted in Figure 14. It takes several minutes until the latent image decays. It was expected that MBE material would not exhibit any persistence. This cannot be confirmed with the engineering grade array tested here.

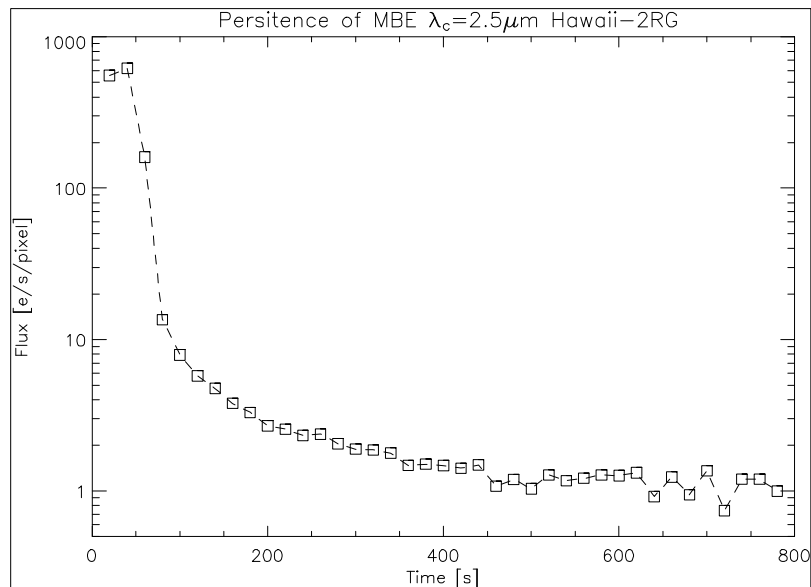


Figure 14 Persistence of Hawii-2RG MBE array in J band. Detector integration time 20 s.

10. Hawaii-2RG in the SPIFFI integral field spectrometer

The first deployment of the Hawaii-2RG array is now being implemented in SINFONI, which combines ESO's curvature adaptive optics system (MACAO type) with an integral field spectrograph SPIFFI [11]. SPIFFI was equipped with a 1Kx1K Hawaii1 array and has now been upgraded with a new camera using a 2Kx2K $\lambda_c=2.5\ \mu\text{m}$ Hawaii-2RG array. In the old configuration with the Hawaii1 array the full spectral resolution required to avoid atmospheric OH emission lines, was only accessible through the spectral dithering technique. This places stringent requirements on the instrument stiffness. In order to relax the requirements on the camera, a 2Kx2K detector and a new camera were mounted in SPIFFI which allow to directly access the full spectral resolution without dithering.

The left image of Figure 15 shows the detector as it is mounted in the instrument. The detector enclosure is electrically insulated from the instrument. This allows grounding of the detector module in a controlled way to the common ground point in the IRACE backplane thus avoiding ground loops and pickup noise. The detector is cooled by copper straps which are thermally connected to the cold camera structure. Clock, video and bias cables are flexible copper boards which are heat-sunk both at the bottom of the cryostat where they enter the light tight enclosure and at the detector enclosure. Since the cryogenic system of SPIFFI is based on a nitrogen bath cryostat the minimum achievable detector temperature is not lower than $\sim 90\ \text{K}$ mainly because of the heat dissipation of the cryogenic preamplifiers.

The right image in Figure 15 shows the spectrum of a Neon calibration lamp in K band taken with an objective which has a pixel scale of $0.1\ \text{arcsec}/\text{pixel}$. The spatial direction is horizontal and the spectral direction is vertical. The spectra of different slitlets are staggered due to the rearrangement of the slitlets by the image slicer. FWHM is 1.4 pixels and the spectral resolution is 6300.

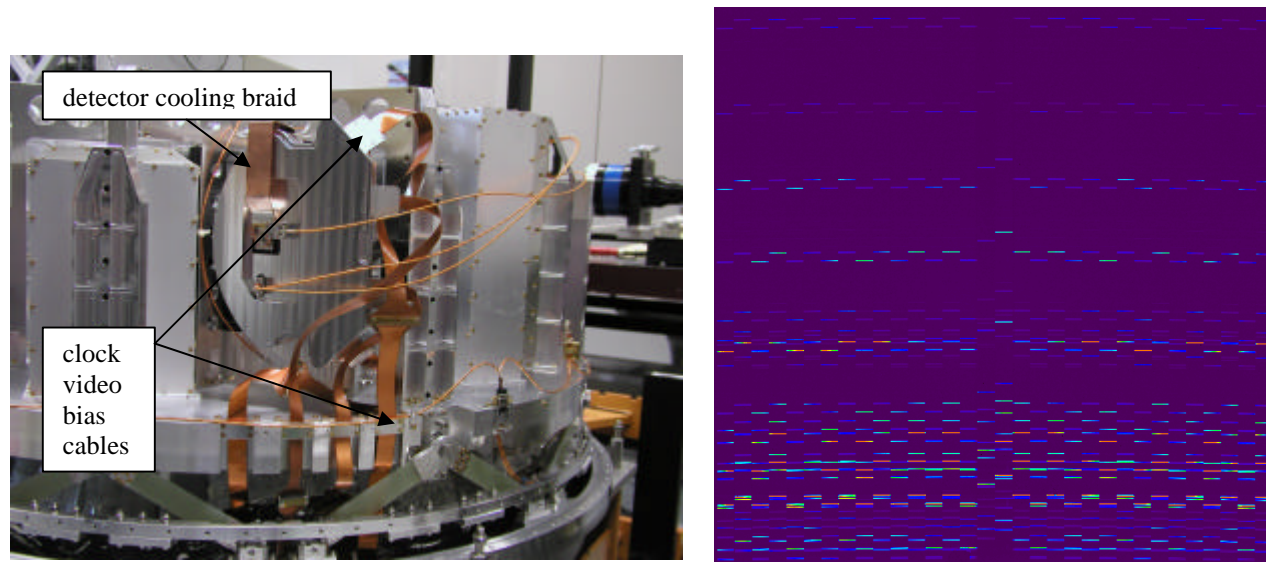


Figure 15 Left: Hawaii2RG array mounted in SPIFFI spectrometer. Right: K band spectrum of Ne lamp

11. Conclusions

The quantum efficiency of MBE-grown HgCdTe on a CdZnTe substrate having a cut-off wavelength of $\lambda_c=2.5\ \mu\text{m}$ is as high as 86% in K and, unlike LPE material, does not drop at lower temperatures. The readout noise of the Hawaii-2RG MBE array is higher (17 erms) than the noise measured with LPE Hawaii2 and the Hawaii1 arrays (10 erms). However, the shielding of the multiplexer glow is very efficient and allows using 256 Fowler pairs. This reduces the readout noise to 3 erms. Cryogenic CMOS preamplifiers at the focal plane do not limit the performance even if used in bath cryostats.

Embedded reference pixels are an excellent tool to suppress low frequency pick-up. A $\lambda_c=2.5 \mu\text{m}$ science grade array can be operated at liquid nitrogen temperature with dark current levels $< 0.01 \text{ e/s}$, provided that the array is free of regions showing excess dark current. This is a substantial improvement induced by changing the growth technology from LPE/ Al_2O_3 to MBE/ CdZnTe . The cosmetic performance of regions with excess dark current improves substantially when the array is cooled to lower temperatures. If sufficient cooling power is available, operating temperatures below 80 K improve the performance of arrays which are not perfect science grade devices. Glow centers generated by large numbers of nondestructive readouts also freeze out at temperatures $< 60\text{K}$. The first Hawaii-2RG array is just being integrated in the integral field spectrometer SPIFFI on Paranal to obtain first light on UT4 at the beginning of July 2004.

REFERENCES

1. J. Pirard, M. Kissler-Patig, A. F. M. Moorwood, B. Delabre, G. Huster, B. Sokar, J. Lizon, A. Silber, D. Gojak, P. Biereichel, E. Pozna, J. Stegmeier, L. Mehrgan, R. J. Dorn, G. Finger, Y. Jung, "HAWK-I: a wide-field near-infrared imager for the VLT", Proc. the SPIE, Volume 5492, to be published.
2. F. Eisenhauer, M. Tecza, N. Thatte, C. Iserlohe, A. Schegerer, J. Schreiber, R. Abuter, M. Horrobin, R. Genzel, H. Bonnet, "On-sky performance of SPIFFI: the integral field spectrometer for SINFONI at the VLT", Proc. the SPIE, Volume 5492, to be published.
3. N. Thatte, I. Lewis, J. Lynn, W. Lau, S. Yang, M. Wells, "A design study for the KMOS spectrograph module", Proc. the SPIE, Volume 5492, to be published.
4. J. D. Garnett, Zandian M., R.E. DeWames, M. Carmody, J.G. Pasko, M. Farris, C.A. Cabelli, D.E.Cooper, G. Hildebrandt, J. Chow, J. T. Montroy, J. Arias, J. Bajai, K. Vural, D.N.B.Hall, "Performance of 5 micron, molecular beam epitaxy HgCdTe sensor chip assemblies (SCA's) for the NGST mission and ground based astronomy", Workshop on Scientific Detectors for Astronomy, pp. 59-79, Kluwer, 2004.
5. M. Loose, Markus, M.C. Farris, J.D. Garnett, L. J., L. J. Kozlowski, "HAWAII-2RG: a 2k x 2k CMOS multiplexer for low and high background astronomy applications", Proc. SPIE 4850, pp. 867-879, 2003.
6. G. Finger, R. J. Dorn, H Mehrgan., M. Meyer, A.F. M. Moorwood and J. Stegmeier, Workshop on Scientific Detectors for Astronomy, "Test Results with 2Kx2K MCT arrays", Workshop on Scientific Detectors for Astronomy, pp. 59-79, Kluwer, 2004.
7. G. Luppino, GL Scientific, private communication.
8. G. Finger, R. J. Dorn, A.W. Hoffman, H. Mehrgan., M. Meyer, A.F. M. Moorwood and J. Stegmeier, Workshop on Scientific Detectors for Astronomy, "Readout Techniques for drift and low frequency noise rejection in infrared arrays", Experimental Astronomy, v. 14, Issue 2, p. 117-127, 2002.
9. M. Loose, L.Lewyn, H. Durmus, J.D. Garnett, D.N.B. Hall, A. B. Joshi, L.J. Kozlowski, I. Ovsianikov, "SIDECAR low-power control ASIC for focal plane arrays including A/D conversion and bias generation", Proc. the SPIE, Volume 4841, pp. 782-794, 2003.
10. D. Figer, STCSL, private communication.
11. F. Eisenhauer, R. Abuter, K. Bickert, F. Biancat-Marchet, H. Bonnet, J. Brynnel, R. Conzelmann, B. Delabre, R. Donaldson, J. Farinato, E. Fedrigo, R. Genzel, N. Hubin, C. Iserlohe, M. E. Kasper, M. Kissler-Patig, G. Monnet, C. Roehle, J. Schreiber, S. Stroebele, M. Tecza, N. A. Thatte, H. Weisz, "SINFONI - Integral field spectroscopy at 50 milli-arcsecond resolution with the ESO VLT", Proc. SPIE 4841, pp. 1548-1561, 2003.